ABSTRACT

EXPERIMENTAL METHOD FOR MEASUREMENTS OF TIME-RESOLVED REFLECTANCE IN A SCATTERING MEDIA

by JIJUN CHEN

When a pulse of light propagates through scattering media, the temporal information of the light carries can be used to extract the optical properties of the media. To achieve this goal, we used a supercontinuum laser source with a time-correlated single-photon counting (TCSPC) based coupled to a single-photon avalanche diode (SPAD) to measure the time-resolved reflectance signals using fibers. This thesis focuses on building an optimal set-up for the measurement by measuring the instrument response function (IRF) and the distribution for photon time of flight (DTOF). To find the optimal set-up, which has the IRF that is consistent with the manufacture and show the difference of DTOF of medium with different optical properties, we not only collected the data from different detectors but also collected it from set-up with different optical configurations and with different fiber probes. Finally, we measured signals from solid tissue phantoms and deduced its optical properties of it using diffusion theory. Preliminary results indicate that data are well modeled by theory. In the future, this system can be used to measure signals from real biological tissues and extract their optical properties.

EXPERIMENTAL METHOD FOR MEASUREMENTS OF TIME-RESOLVED REFLECTANCE IN A SCATTERING MEDIA

Thesis

Submitted to the

Faculty of Miami University

in partial fulfillment of

the requirements for the degree of

Master of Science
by

JIJUN CHEN

Miami University

Oxford, Ohio

2018

Advisor: Dr. Karthik Vishwanath

Reader: Dr. Samir Bali

Reader: Dr. Paul Urayama

This Thesis titled

EXPERIMENTAL METHOD FOR MEASUREMENTS OF TIME-RESOLVED REFLECTANCE IN A SCATTERING MEDIA

by

JIJUN CHEN

has been approved for publication by

College of Arts & Science

and

Department of Physics

_____

Dr. Karthik Vishwanath

_____

Dr. Samir Bali

_____

Dr. Paul Urayama

Table of Contents

List of Tables

List of Figures

Dedication

Passion of unknown guides everything

Acknowledgements

Thank physics department of Miami University, professor Vishwanath, and McMaster, Carter.

1.Introduction

When a photon travels through a turbid medium (such as biological tissues), it can be absorbed or scattered by it [1]. The scattering and absorption are determined by the medium's optical properties. There are three parameters that describe these phenomena – the absorption coefficient, the scattering coefficient and the anisotropy coefficient are used to describe tissue optical properties. The absorption coefficient μ_a cm^{-1}, represents that when a photon travels through a media over an infinitesimal distance ds, the probability of absorption is $\mu_a ds$. The reciprocal of μ_a also is referred to as the absorption mean free path [1, 2]. The scattering coefficient μ_s, defines that the probability of a photon that is scattered when it travels through a media over an infinitesimal distance ds is $\mu_s ds$. The reciprocal of μ_s is referred to as the mean absorption length. The extinction coefficient μ_t is defined as the sum of the absorption coefficient and scattering coefficient. The anisotropy coefficient g, is the average value of $cos\theta$, where θ describes the angle of deflection for a single scattering event. The reflectance measured in tissue depends on these three parameters which depend on the wavelength of light[1]. Here, we propose an experimental strategy to obtain tissue optical properties using experimental measurements.

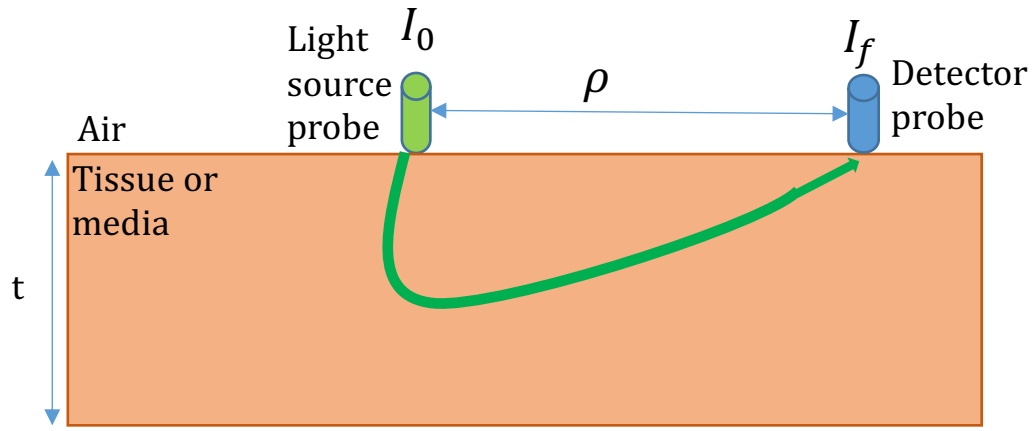

Figure 1: light transport through the semi-infinite media. The photons come from the light source probe can be absorbed or scattered by the media. The green line represents one of the examples how photons are captured by the detector probe. How photons be absorbed and scattered depends on the optical properties of the media.

As figure 1 shows, the light source comes from the light source probe and travels through the media or tissue. $I_0$is initial light intensity, ρ is the distance between the light source probe and detector probe. The t represents the thickness of the media or tissue. I_f represents the light intensity that received by the detector. The photons can be scattered or absorbed by the media and then some photons will be collected by the detector. The green curve in figure 1 is one of particular paths for remitted photons. The light intensity collected by the detector can be function of thickness, absorption coefficient, scattering coefficient, anisotropy of media, the distance between the light source probe and detector probe, and the light source[3, 4].

Reflectance is referred as the fraction of incident power that is reflected at an interface. There are several ways to get the optical properties of tissue by the measurement of reflectance[5], depending on the type of light source used in the measurement. The first type of light source is the continuous wave light source, which means intensity of light source doesn't change with time, $I(t) = I_0$. When we use this type of light source, it is referred as the steady-state method measurement. And the light intensity that received by detector I_f is the function of μ_s, μ_a, g, ρ[1]. The second type of light source is pulse laser light source. It is also referred as the time-resolved measurement[6], which implies the intensity of light source is changing with time and the remitted light signal I_f is the function of μ_s, μ_a, ρ, g, t[7].

1.1 Steady-state method

Using a continuous wave light source as light source, as well as the spectrophotometer as the detector, the steady-state method measures the reflectance of the medium as the function of wavelength[8]. Experimentally, it typically requires at least three measurements in order to derive optical properties of an unknown medium[8]. These being a measurement of the spectral output of the light source, the diffuse reflectance spectrum of the medium of interest and last a measurement of the diffuse reflectance spectrum from a "calibration" phantom with known optical properties. Even then, the uncoupling result of the absorption coefficient and scattering coefficient makes the measurement tedious[1].

However, the overall cost of steady-state method ranges from hundreds to thousands of dollars and is by far the most low-cost method to derive optical properties from diffuse reflectance [9, 10].

1.2 Time-resolved method

Compared with steady-state method, time-resolved method does not need any assumption. It provides the richest information and we can extract the optical properties directly[11]. Using time-resolved method, we can obtain $\mu_a$and $\mu_s$from a single distance measurement by analyzing the shape of the distribution time of flight of photons (DTOF) since the μ_a and μ_s affect differently the photon time distribution. The higher absorption coefficient, the lower of DTOF. The higher scattering coefficient, the more broadening of DTOF. However, time-resolved instrumentation is expensive typically requiring ultra-fast (pico-femto second) light sources dollars and time-resolved detectors capable of resolving time-of-flight with pico-second resolutions[12].

Because light transport is a fast phenomenon, usually around 100 ps, in order to get the temporal response of media, we need an ultra-fast pulsed light source (attoseconds to nanoseconds). Here we use ultra-fast supercontinuum laser source. Additionally, since such measurements also require detection on picosecond scale, appropriate time-resolved detector systems are needed. Here, we use a time correlated single photon counter (TCSPC) system with avalanche photon detector(APD) [13].

1.3 Motivation and aims

Time-resolved spectroscopy of diffuse media has been widely used as both research and diagnostics tool to assess optical properties of tissue. For example, it can provide the insight of the blood flow change, the concentration of the oxygen and various chromophores in a noninvasive method[14, 15].

The main aim of my thesis is to present an experimental method to extract the optical properties of the medium by measuring the time-resolved reflectance. Knowing the optical

properties of the media or biological tissue can help us to understand the tissue or the media better. By the end of the work, we showed how we built the optimal set-up to measure the DTOF of solid phantom. We showed that the absorption filter and the detector itself can cause the diffusion tail in IRF measurement. Based on the polarizers, mirrors and fiber, we built the optimal set-up to measure the solid phantom. The result of the IRF convolved with the diffusion theory matched with our measurement of the DTOF of the solid phantom.

2.Theory

2.1. Diffusion theory

When the optical scattering of the medium is much greater than the absorption coefficient and if the emitted photons have undergone many scattering events, photon transport can be approximated as a diffusion equation[16]

$$\frac{\partial \phi(\vec{r},t)}{\partial t} = c[D\nabla^2\phi(\vec{r},t) - \mu_a(\vec{r})\phi(\vec{r},t) + s'(\vec{r},t)] \quad (1)$$

In equation (1) $\phi(\vec{r})$represents the photon fluence rate at position $\vec{r}$ (within the medium) and represents the power carried by the photons per unit area. c is the speed of light. D is diffusion coefficient, which is related to absorption coefficient, scattering coefficient and anisotropy coefficient. It can be expressed as[12, 16],

$$D = \{3[\mu_a + (1-g)\mu_s]\}^{-1} \quad (2)$$

$s'(\vec{r},t)$ is an arbitrary fluence term, to account for the photon source. For an isotropic point source $s'(\vec{r},t)$ is a delta function $\delta(\overrightarrow{r_0},t_0)$. By using Green's function and inverse Laplace transform, equation (1) can be solved for an infinite medium to give[1, 6, 17]:

$$\phi(\vec{r},t) = \frac{c}{(4\pi Dct)^{\frac{3}{2}}} exp\left(\frac{-r^2}{4Dct}\right) exp\,(-\mu_a ct) \quad (3)$$

However, the equation (3) is the solution for the infinite medium. For the solution of semi-infinite medium, it needs two boundary conditions. The first boundary condition is that the fluence is zero at infinity. The second one is that photons only come from the media inside, which can be expressed in mathematically [18]:

$$\phi(\mathrm{r}) - 2AD\widehat{\Omega}\cdot\nabla\phi(\mathrm{r}) = 0 \quad (4)$$

$\widehat{\Omega}$ is a unit normal vector directed into the medium (usually also taken to be the direction of the incident light). Equation (4) can be satisfied by letting the fluence ϕ equal to zero at some extrapolated boundary above the surface of the medium and is called as extrapolated-boundary condition (EBC) [19]. The height of this extrapolated boundary, is set to be

$$z_b = 2AD \quad (5)$$

A is the coefficient that relates to the relative refractive index of the two media and critical refractive angle. When the refractive of two media is equal, A=1.[18]

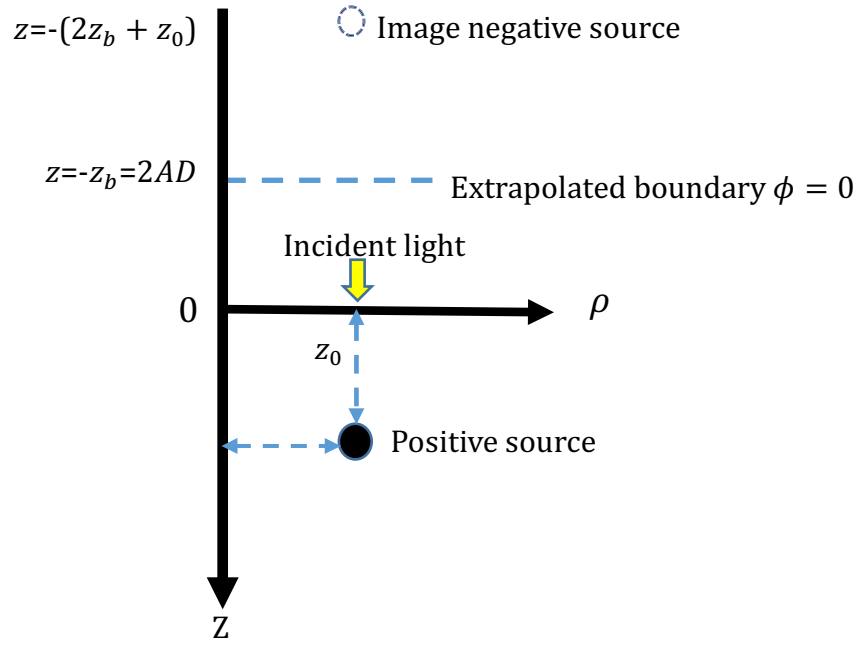

Figure 2 Schematic figure for boundary condition to model photon diffusion from a collimated source into semi-infinite media. This boundary condition can be achieved by introducing an image negative source above the semi-infinite media.

As it is shown in figure 2, ρ represents the radial distance and z represent the distance normal to the medium surface of the blue point. The yellow arrow represents that the light shines on the media surface and the distance of blue point to the surface of the media is z_0. It is regarded as the first being scattered photon.

$$z_0 = [(1-g)\mu_s]^{-1} \tag{6}$$

The fluence at depth within the media can be forced to zero on a plane by introducing a negative 'image source' as the dash circle is shown in Figure 2 [18]. For a photon source within the medium at z_0 and the height of the extrapolated boundary z_b, the distance from the extrapolated boundary surface to the photon source is z_b+z_0. The image source will be at the height of z_b+z_0 above extrapolated boundary so that the fluence rate will be cancelled out and be zero. Thus the position of the image source will be a height of $2z_b+z_0$ above the media surface.

Changing the variable r of equation (3) into radial distance ρ and the distance normal to the boundary z, we get

$$\phi(\rho,z,t) = \frac{c}{(4\pi Dct)^{\frac{3}{2}}} exp(-\mu_a ct)\left[exp\left(\frac{-(z-z_0)^2+\rho^2}{4Dct}\right) - exp\left(\frac{-(2z_b+z_0+z)^2+\rho^2}{4Dct}\right)\right] \tag{7}$$

$\vec{F}(\vec{r},t)$, the diffusion flux vector at position $\vec{r}$ and indicates the energy of light per unit area and per second, is related to diffusion coefficient and fluence rate by Fick's law definition. Therefore,

$$\vec{F} = -\mathrm{D}\overline{\nabla}\phi(\rho,z,t) \tag{8}$$

We have the equation to calculate the reflectance at position $\vec{r}$ on the surface of the media[17]

$$R(\rho,z=0,t) = \frac{1}{4\pi}\phi(\rho,z=0,t) - \frac{3}{4\pi}\mathrm{F}(\rho,z=0,t)$$
$$= \frac{3}{2(4\pi Dc)^{3/2}t^{5/2}} \cdot \exp\left(-\mu_a ct - \frac{{z_0}^2+\rho^2}{4Dct}\right) \tag{9}$$

3.Experimental method

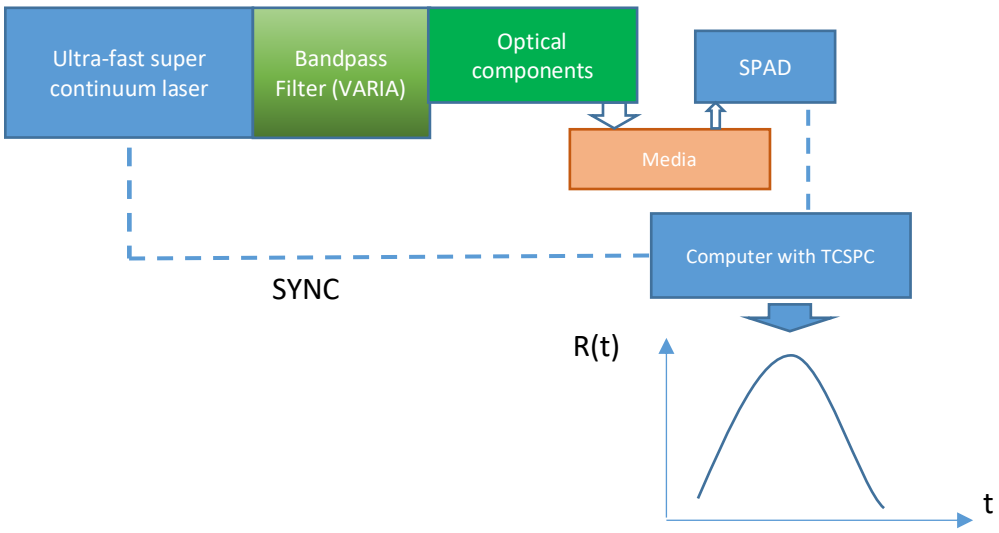

Figure 3 A schematic of set-up. The light come from the laser source pass through the bandpass filter and controlled by the bandpass filter. Then it will pass through optical components such as glass, an absorption filter, polarizer, mirror, fiber. The free space set-up is referred to the absence of any optical component in a set-up. The light travels through the media will be captured by the detector SPAD. The dash line represents the electronic signal and the white arrow represents the optical paths. Finally, the computer with TCSPC system can yield the time-resolved reflectance of the media.

Figure 3, shows a schematic of the experimental set-up. The ultra-fast super continuum laser sends the light into the bandpass filter. The bandpass filter can control the bandwidth and the central wavelength of the pulse. Between the bandpass filter and media, there could be different optical components such as mirror, glass, polarizers and filter involved in the path and we built twelve set-ups with different optical components as table 1 shows. The light that comes from the laser source travels through the media and they are captured by the avalanche photodiode(APD). Here, we have two types of APD detectors(ID100, IDQ, USA)(PDM, MPD, USA)and we used both of them in the experiment. The TCSPC system on computer collects the temporal information from synchronization (SYNC) signal from the laser source and intensity of the emitted light from the detector. Because the detector yields the intensity as the function of the time and the reflectance is defined as the fraction of the input intensity detected at the surface of the medium from the source, we can get the time-resolved reflectance of tissue based on this system. Before using this system to measure any media, the most important thing is to measure the instrument response function (IRF) from the laser, which means the detector read directly from the laser source. The pulse width shown in the IRF should be consistent with the manufacturer of the laser source. Given that, we can measure the time-resolved reflectance of the media or distribution time of flight(DTOF) of the media.

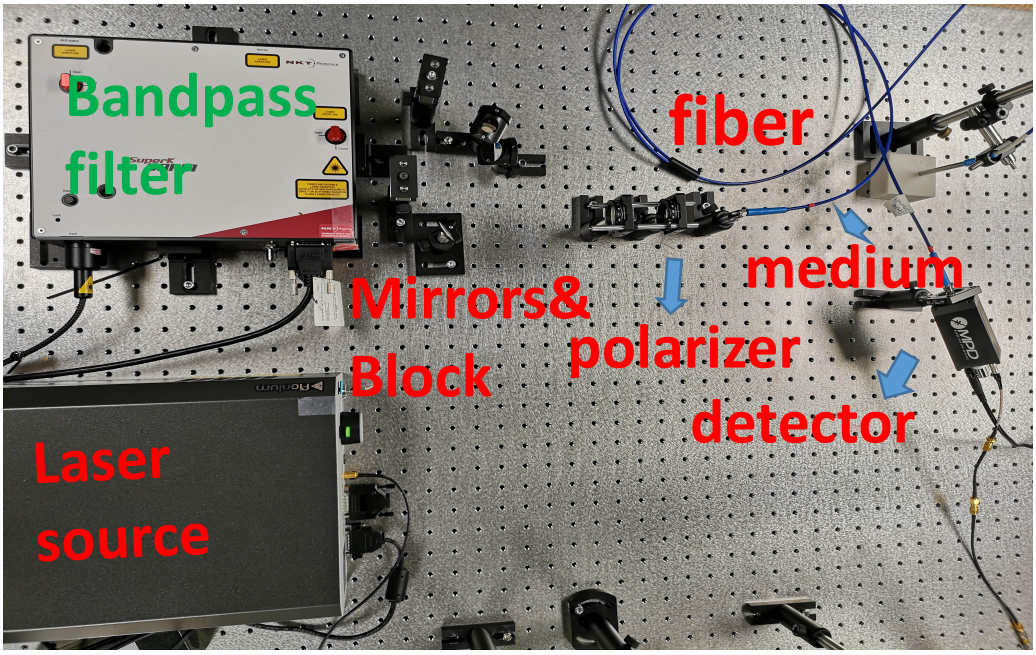

Figure 4 Lab set-up. It shows one of the examples of what optical components can involve in, which are mirrors, polarizers and fiber. The light passes through the optical components and goes into the fiber probe. Then the fiber probe sends the light into the solid phantom and remitted light goes to the detector.

Like figure 4 shows, the light coming out from the bandpass filter is directed to two of parallel mirrors, which can raise the light beam to certain height. Then it passes through the polarizers which can decrease the intensity of the light and shine into the blue fiber probe. The path from the bandpass filter to the medium can have many optical combinations such as the absorption filter, reflected filter, polarizer, mirror, different types of fibers, glass, lens. Our main goal is to focus on which optical combinations are the optimal set-up for the reflectance measurement.

Set-up Number	Optical components in Figure 3
Set-up 1	Absorption filters and fiber
Set-up 2	Absorption filters and glasses
Set-up 3	Only absorption filters
Set-up 4	Free space
Set-up 5	Absorption filters and mirrors
Set-up 6	Only polarizers
Set-up 7	Only fiber
Set-up 8	Polarizers and mirrors
Set-up 9	Polarizers, mirrors and reflected filter
Set-up 10	Polarizers, mirrors and two-patch fiber
Set-up 11	Polarizers, mirrors and bundle fiber
Set-up 12	Polarizers, mirrors and black-4-channel-DRS fiber probe

Table 1 Optical components included in the set-up. We use different optical components in set-up and see how the affect the measurement.

3.1 Light Source and Bandpass Filter

There has been lot of research that aimed to get time-resolved reflectance measurement of biological tissue using supercontinuum laser, photomultiplier tube(PMT) or avalanche photodiode(APD) as the detector and time-correlated single photon counting (TCSPC) system[5, 20-26]. Here we present the way to get the optical properties of the solid phantom experimentally. First, ultra-fast super-continuum laser, as the light source, works by sending an ultrashort, high-energy pulse in at 1040 nm though a non-linear fiber (photonic crystal fiber) [27], which then emits a supercontinuum pulse with wavelengths ranging from 400nm to 900nm. It would allow for making time-resolved measurements across visible light through near-infrared spectrum from 400 nm to 900 nm. Thus, we can probe the time-resolved reflectance of turbid scattering samples from across a wide range of wavelengths of light. We expected the pulse width of our laser source to be ~100ps (across this whole spectrum) and had a repetition rate of 40MHz. The average pulse energy from 400 nm to 750 nm is about 10 μJ. These are the features provided by the manufacturer.

However, in order to make sure the laser source and bandpass filter is controllable over the computer, it needs to be tested how the spectrum looks like for the laser light come from the bandpass filter.

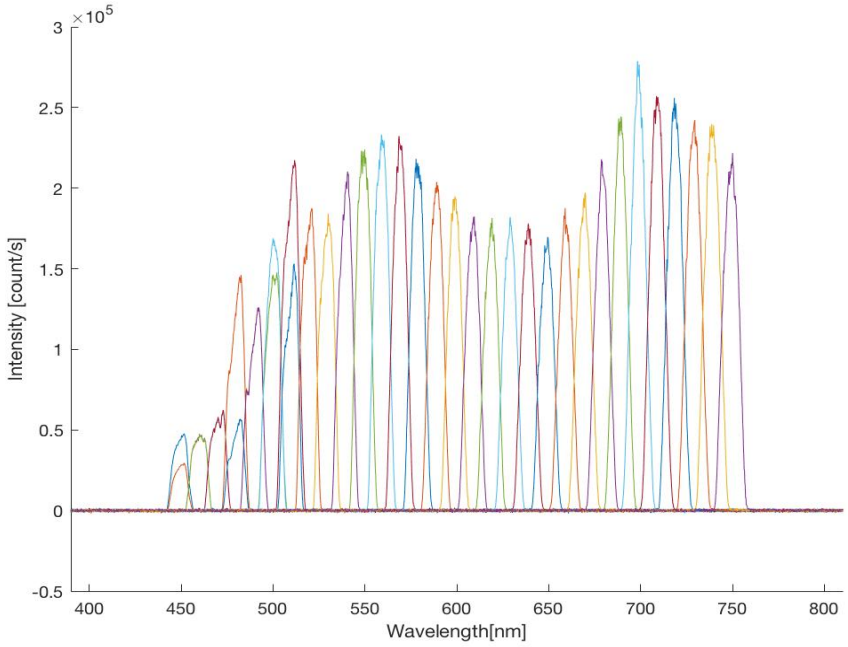

Figure 5 The spectrum of the laser source came from bandpass filter. The Bandpass filter can control the bandwidth and central wavelength of the light from the laser source. We collected this data with central wavelength from 450nm to 750nm and with the same 10nm bandwidth.

As it shows in figure 5, in order to make sure the laser source spectrum look exactly like what we expect, we measured the spectrum of the laser source using a standard spectrometer (<USB4000>, Ocean Optics, USA). For these measurements, we coupled a fiber to the spectrometer, and coupled the other end to the output of the bandpass filter SuperK Varia (NKT

photonics, USA). Figure 5 shows different central wavelengths will have different light intensity and they were all collected in 10 nm bandwidth. This test can make sure bandpass Super K can control the central wavelength and the bandwidth of the laser source.

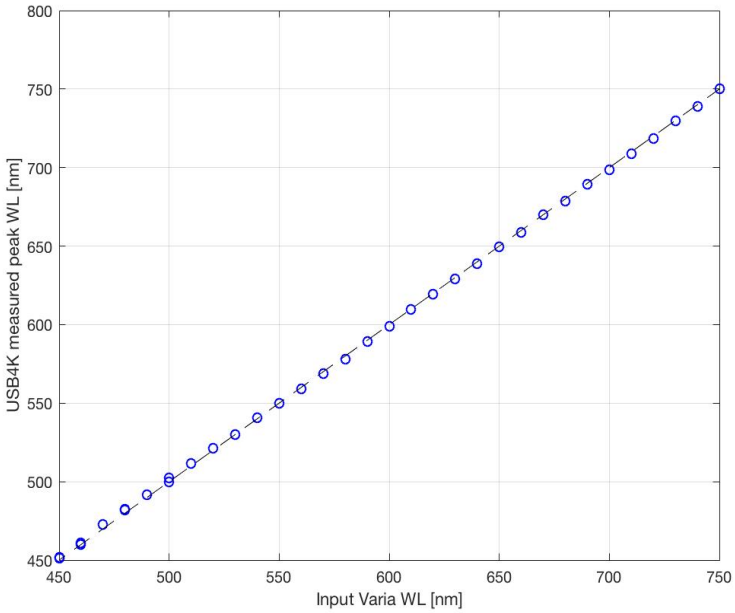

Figure 6 Peak wavelength measured versus wavelength chosen on bandpass filter, which is close to a linear relationship.

Again, we let the light come from the bandpass filter shine into the spectrometer directly and made figure 6 as the specific wavelengths we selected in bandpass filter as x axis and the output of spectrometer as y axis. Figure 6 showed the linearity between the peak wavelength measured versus the wavelength chosen on bandpass filter, which proved the bandpass filter can yield the central wavelength of light we wanted.

3.2 TCSPC system

When it comes to laser-related measurement, we need a system that can not only meet the accurate time resolution (laser pulse width is about 100 picoseconds) requirement but also it is able to accumulate enough photons to create an analog voltage representing specific optical flux(The optical signal may consist of just a few photons per cycle) [28]. TSCPC system can solve these questions by extending the data collection over multiple cycles. If we can meet the requirement of sparseness of the collected photons, it is possible for us to reconstruct the pulse profile from the multitude of single photon events over many cycles)[29].

TSCPC gets the timing information from the measurement of the time differences between the single-photon pulse from the detector and reference pulse which come from synchronization (SYNC) signal. Due to the amplitude jitter of pulse and timing jitter, the constant-fraction discriminators(CFD), are used both at the detector and at the reference input. The mechanism of CFD is creating zero crossing point which is independent of amplitude.

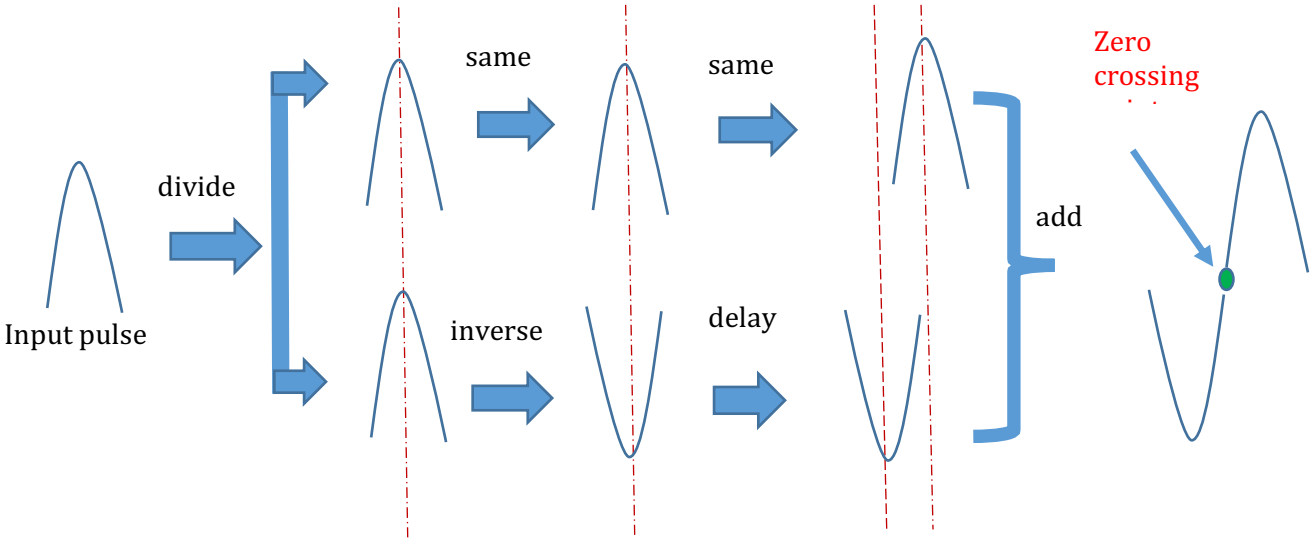

Figure 7 The mechanism of CFD. When the light signal reach the CFD, it will divide into two signals. One will keep the original pulse and another will invert the original signal pulse and delay it. Adding up these two signals can create the zero crossing point of the input pulse and the inverted and delayed input pulse.

The zero crossing point of the CFD make the optical events are easy to be detected for electronic device. Also, there is another reason for using CFD. CFD contains a discriminator select the pulse, which can reject the noise from environment partly. The delay control of CFD is realized by changing the length of SYNC signal.

The TCSPC system works by collecting the average of many impulse intensities for every single time bin from APD so that it can reconstruct the profile of the pulse from the multitude single photon events over many cycles. The most important thing is guaranty that there is only single photon for single time bin. Noted that there is 'dead time' between the detector and electronic device, which describe the system cannot register photons while it is processing a previous photon event, so it is necessary to maintain a low possibility of registering more than one photon per cycle. This condition can be met by attenuating the light level.

The single photon detector must have a suitable gain mechanism so that it can deliver a significant output pulse for single detected photon and at the same time the output should be short enough to resolve a single photon event. There are mainly two types of detectors met that requirements, one is based on photon multiplier tube(PMT), another is single-photon avalanche photodiode(APD). Although both may work for the purpose of our studies, we opted to use an APD because due to availability. The APD is an electronic device which is able to detect low intensity signals (usually only one photon) and also signal the time of photon arrival with the high temporal resolution[13].

3.3 Detectors and Methods Tested

3.3.1 ID100

3.3.1.1 ID100 IRF

What we want to get eventually is the optical properties of a medium. We can extract the optical properties from the time-resolved reflectance measurement using the theory. As it mentioned before, in order to get the time-resolved reflectance measurement, we need a supercontinuum laser, a single photon avalanche diode (SPAD) detector and the time correlated single photon counter (TCSPC) system. The module type of SPAD we used first is ID100.

First we tried to get the instrument response function (IRF) from the laser source, because we have to make sure the laser pulse shape looks exactly like a sharp pulse and the pulse width is same with what we are expecting, which should be around 70 ps. Besides, in diffusion theory, it assumes the light source as the point source, so we need the IRF to convolve with the diffusion theory to get the DTOF of the media.

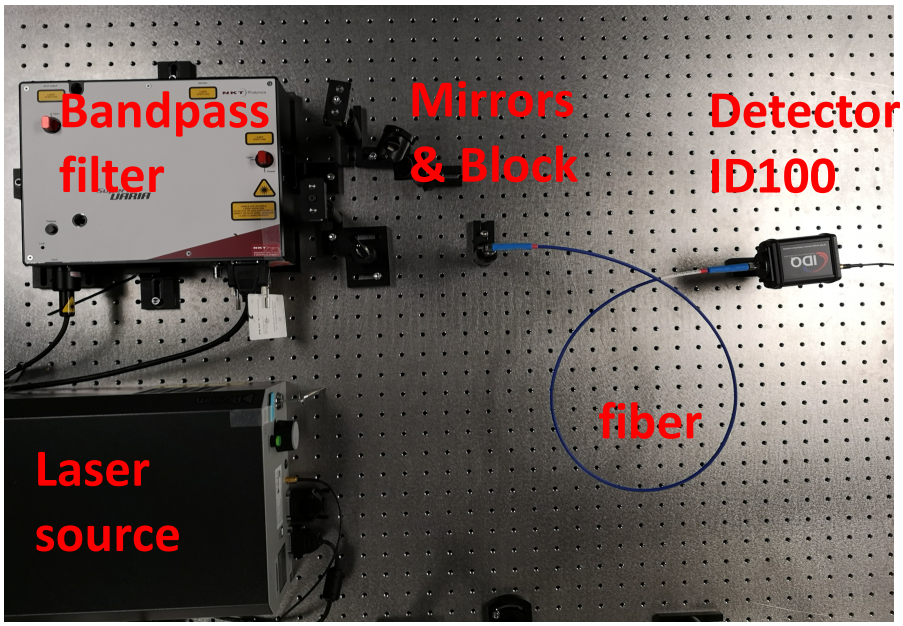

Figure 8 IRF measurement set-up. The optical components included were mirrors and fiber and the APD detector used was ID100.

As the figure 8 shown, the light emerging from the bandpass filter was directly picked up by the fiber which was detected using the ID100 detector. The reason why we want to use fiber is that we want to keep the dark count rate as low as possible. The fiber coupled into the detector can keep the detector from collecting photons from background so that it only collects the photons signal that came from the laser source.

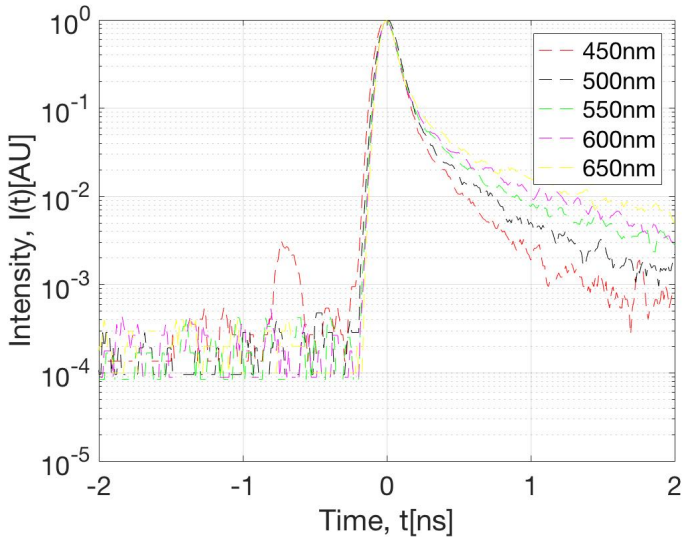

Figure 9 IRF from 450nm to 650nm with 10nm bandwidth for the set-up 1 in table 1. These IRF are suffered from diffusion tail.

We are expecting the IRF of the laser source looks like a Gaussian function, however, what we observe is the broadened tail of the IRF. This kind of tail can also be referred as diffusion tail[13]. The diffusion tail was present for wavelengths from 450nm to 650nm. The 450 nm IRF includes some noise because of too low CFD values. Also the shape of the IRF should be as sharp as possible and the FWHM of IRF should be corresponded with the laser pulse width, which is around 60ps.

In order to check if the diffusion tail was caused due to temporal dispersion by fiber, we built the set-up 2 by coupling the laser light (after attenuation) as shown schematically in figure 10. The light intensity is cut down by glass and filter. The glass only reflects 4% of light. Changing the OD value of filter can be used to control the CFD value. We collected the IRF again based on this set-up.

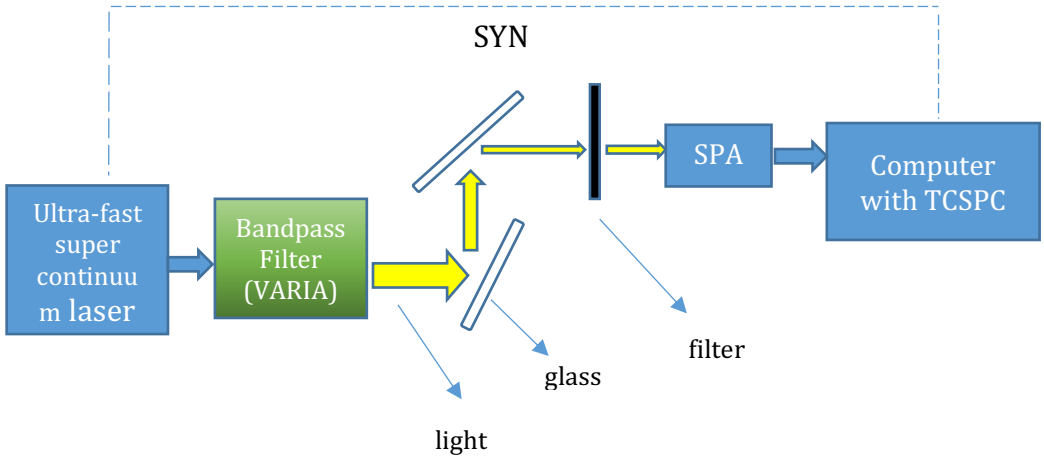

Figure 10 Set-up 2 in table 1. The optical components involved in were glass and filter.

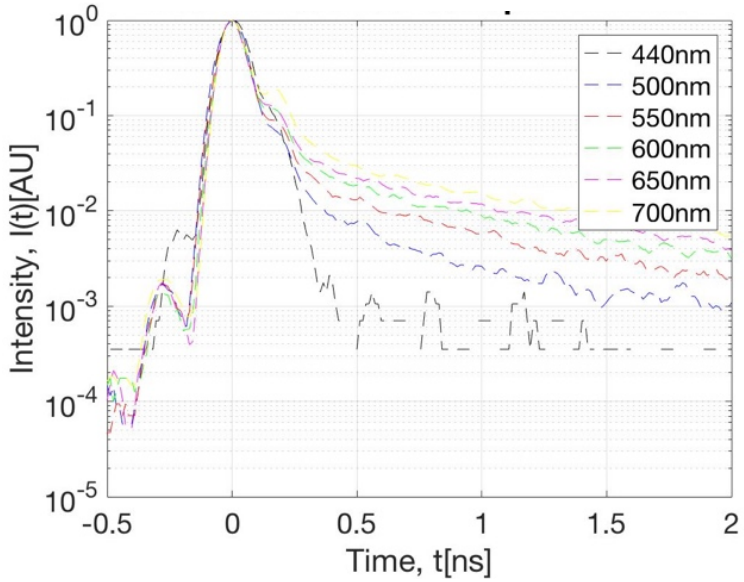

Figure 11 IRF of set-up 2 in table 1 from 440nm to 700nm. Only 440nm wavelength IRF was free from diffusion tail. Other wavelength IRF had a severe diffusion tail.

Figure 11 shows the results of these measurements and we can see that only the wavelength below the 450 wavelength was free from diffusion tail. The degree of diffusion tail is increasing as the increase of wavelength, showing the diffusion tail is wavelength-depended.

Next, we wanted to see whether we could improve the diffusion tail by changing the CFD value. So we collected the data with low CFD values and high CFD values at 440nm from set-up 2.

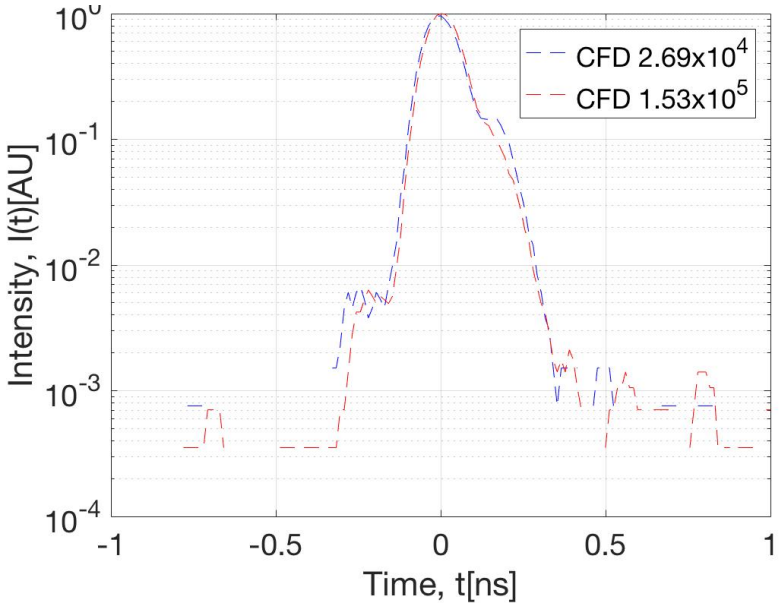

Figure 12 Set-up 2 IRF at wavelength 750nm for different CFD values.

We collected data with different CFD at 440nm. From figure 12, it can be known that the CFD didn't change the diffusion of the IRF for 440nm since the IRF with different CFD values almost overlapped with each other.

The diffusion tail in photodetectors is caused by the photons which penetrate the depletion layer and generate photons in the neutral regions, which is the place outside the hole in P-N junction[12, 26, 30]. This phenomenon usually is wavelength-dependent and so the diffusion tail is also wavelength-dependent. Thus, we concluded that the diffusion tail can be modified by changing the detector module. Because we have two different series of ID100, we want to test whether there are any difference between these two detectors.

3.3.1.2 Comparison between two ID100 detectors

We have two ID100 detectors. Although they are same type of detector, they were made by different manufactures and thus they have different serial numbers. We collected the data from these two ID100 detectors in set-up 2 to see whether they get the same IRF for different wavelengths.

ID100	Dark count rate	Active area diameter
ID100-50	5.2×10^2	50μm
ID100-20	1.22×10^2	20μm

Table 2 The dark count rate and active diameter of two ID100 detectors.

Dark count rate refers to the signal of the detector that doesn't come from the laser source but from the background of the set-up. Although under the same condition and using same type of detector, the dark count rate of these two detector are slightly different. The difference of dark count rate could come from the difference of electronic device inside the detector.

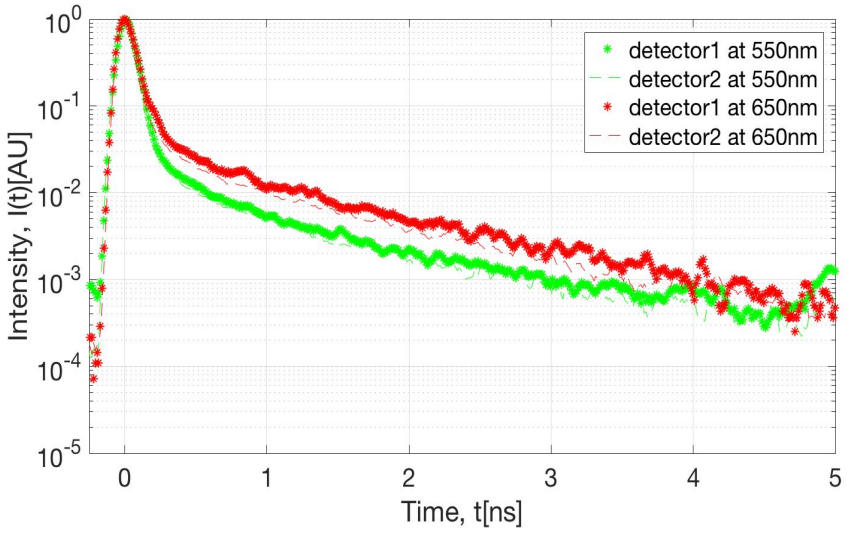

Figure 13 IRF of set-up1 using two different ID100 detectors

There are no difference of IRF at 550nm and 650nm between these two ID100 detectors in figure 13, which means that this type of detector could always cause the diffusion tail in the IRF,

so we continued to use the ID100 to test the reflectance of phantom and tried to find out the which way can get rid of the diffusion tail.

3.3.1.3 Measuring the liquid phantom

Although the IRF suffers from serious diffusion tail, it is unknown that whether it will hamper the attempt to get optical properties of a tissue. So instead of just shining laser source light into the detector, the light will pass through the phantom and the output of this time-resolved measurement is called distribution time of flight (DTOF). We tried to see what we will see from DTOF of liquid phantoms with different scattering and absorption coefficient.

We added a certain amount of dye as the absorber and the milk powder as the scatterer. Since only below 450nm is free from diffusion tail and we wanted the liquid phantom absorbed the light below 450nm as much as possible. We collected the data at 450nm and chose to use the green dye and red dye with a student-made fiber in set-up. We added a certain amount of red dye, the same amount of scattering power and changed the absorption coefficient of the liquid phantom by adding more water. The more water, the lower of the absorption coefficient of the liquid phantom.

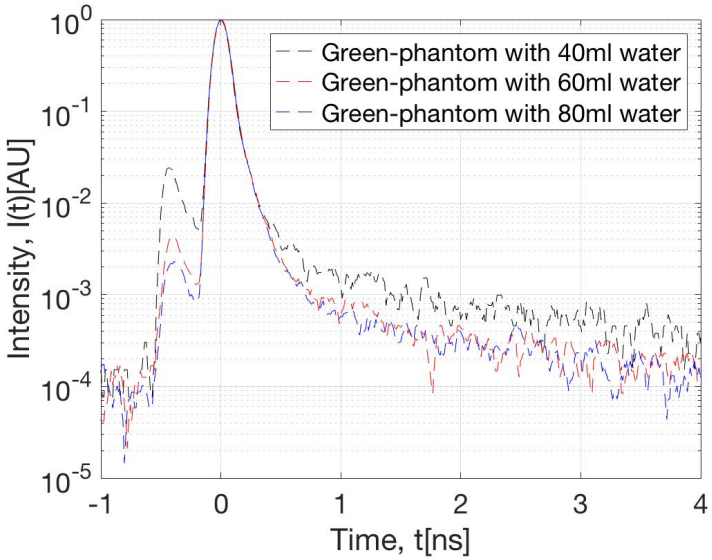

Figure 14 Testing green liquid phantom at 450nm using set-up 1 (1).

With a certain amount of green dye, we changed the absorption coefficient of liquid phantom by changing the volume of water. The liquid phantom with 80 ml volume of water has the highest absorption coefficient since the intensity of it is the lowest and the liquid phantom with 40 ml volume of water has the lowest absorption coefficient since the intensity of it is the highest. The small bump appears a few ns before the main peak is unexpected. It should not show up in the DTOF of the liquid phantoms.

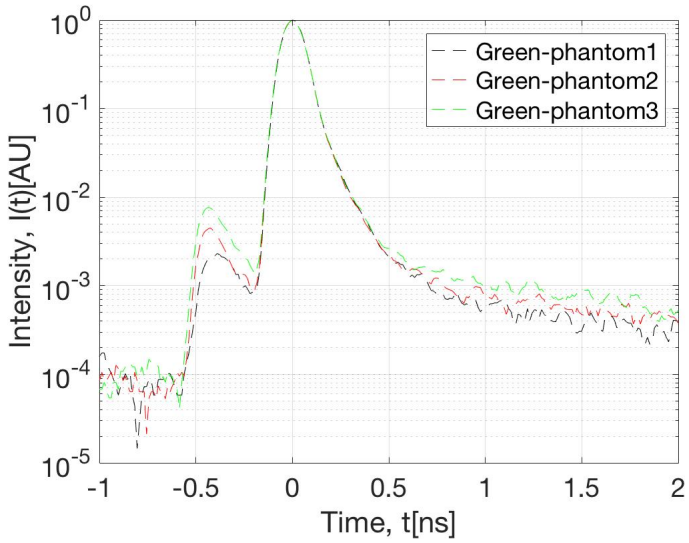

Figure 15 Testing green liquid phantom at 450nm using fiber set-up 1 (2).

Then we compared green dye liquid phantoms at different scattering coefficient under the same absorption coefficient. Figure 15 data is collected from green dye liquid phantoms at 450 nm. The Green-phantom1 has the lowest amount of scattering powder, while Green-phantom2 has the medium volume of scattering powder and the Green-phantom3 has the highest amount of scattering powder. Although the IRF of Green-phantom3 with the highest scattering is the most broadening compared with other two liquid phantoms, the difference is not significant.

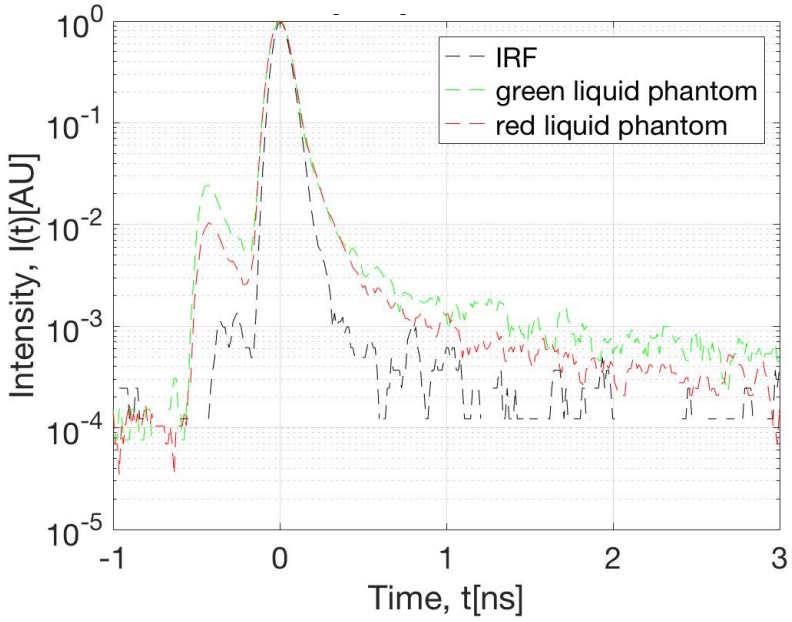

Figure 16 IRF vs DTOF of green and red liquid phantom for set-up 1

Through comparison, it was found that the liquid phantom didn't fit the expectation. Although he DTOF of the liquid phantoms are more broadening compared with their correspond IRF because the photons have undergone many scattering events in DTOF measurement.

However, the DTOF of red liquid phantom and green liquid phantom should not look like the same. Thus, figuring out a way to optimize the set-up is still necessary.

3.3.2 MPD

Compared with ID100, MPD, another type of single-photon avalanche photodiode, has higher quantum efficiency. In order to made sure the new detector MPD is better than ID100, we collected the IRF from these two detectors. The MPD data collect from the free-space and ID100 data collected from the set-up with optical component absorption filter. Through comparison IRF of ID100 VS MPD, we knew that the IRF from MPD is better than ID100 since the IRF measured by MPD is sharper than by ID100, so we decided to use MPD as our detector to build the set-up.

3.3.2.1 Pre-pulse

The pre-pulse is a phenomenon that the bump appears a few ns before the main peak[13]. The pre-pulse showed in the IRF when we were using the MPD detector. There are two reasons that can cause pre-pulse: when photoelectron emission from the first dynode and the corresponding pulse reach the anode prior to the photons from the cathode, it will have a lower amplitude before the real IRF[13]. So we can suppress these pre-pulse by increasing the threshold of the discriminator. It can also occur when an inappropriate zero cross level in CFD. If the zero cross is too close to the signal baseline, the zero cross comparator may oscillate and produce a double structure in the IRF. So again we collected the IRF from MPD with different limit low and ZC level values.

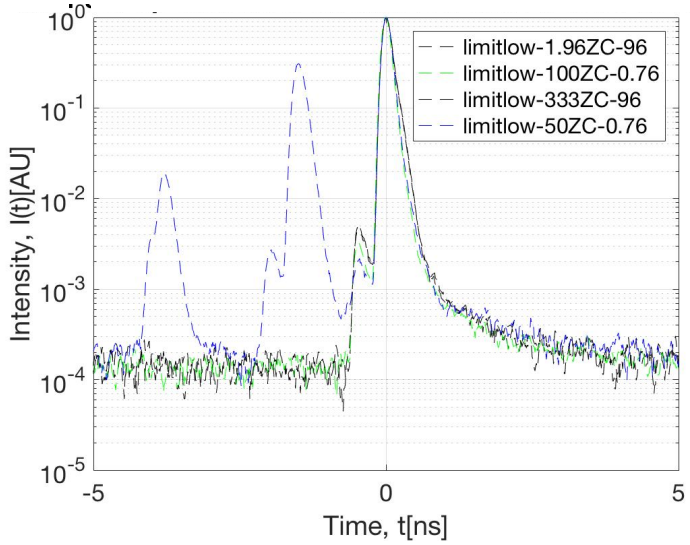

Figure 17 IRF with different limit low and ZC level for set-up 3 in table 1

In figure 17, only the black line with limit low values -333 volts and ZC level -96 vlots are free from pre-pulse. We collected the data with higher or lower limit low and ZC level respectively and it was found that when limit low is above the -50 volts and ZC level is above -96 volts the IRF will always have pre-pulse. When either limit low or ZC level is below these values, the pre-pulse can disappear. We set the limit low and ZC level to the optimal value and kept them at the same value in the afterward experiments.

3.3.2.2 After-pulse

Similar to the pre-pulse, the bump which has less significant intensity than the main peak and appears a few ns after the main peak in IRF called the after-pulse[13]. Usually, after-pulse is caused by electrons and holes from a previous avalanche. The carriers are trapped in lattice imperfections.

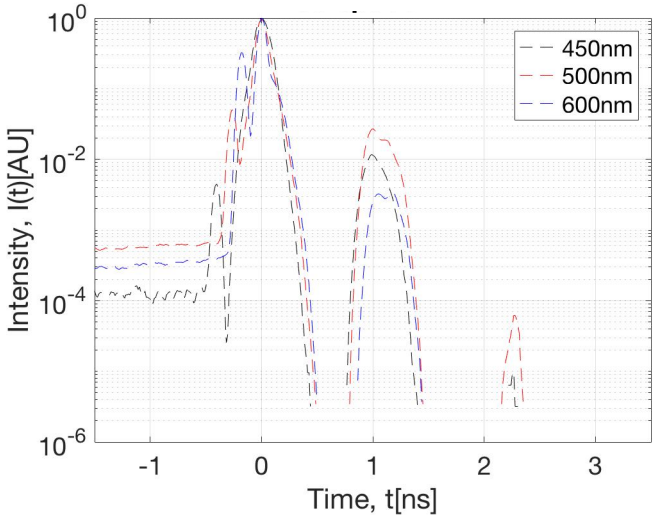

Figure 18 IRF of free space set-up 4 from 450nm to 600nm

Figure 18 shows that although free space set-up 4 IRF is free from pre-pulse and diffusion tail, the after-pulse problem looks serious. All wavelength is suffered from the after-pulse problem. These after-pulse could also come from the reflection of the surrounding object. Because when we used the filter in the set-up, the after-pulse phenomenon disappeared. Setting the filter in the path can cut down the reflection so that we can't see them. So we continued to use the optical components to optimize the set-up.

3.3.2.3 Diffusion tail

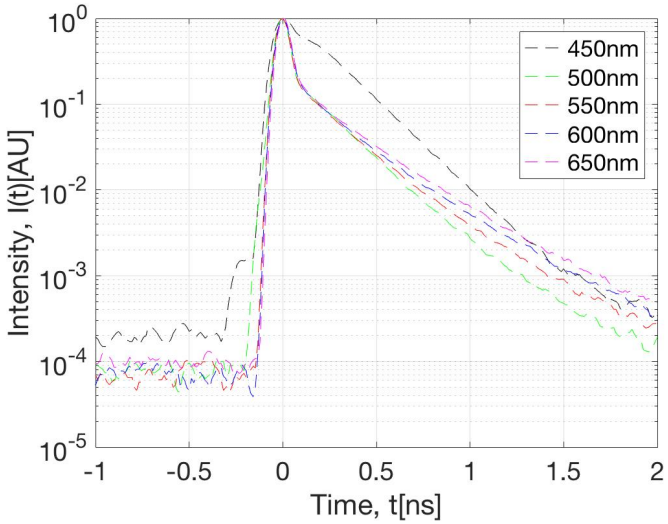

Figure 19 IRF of absorption filter and mirror set-up 5

From 450nm to 650 nm, the IRF of absorption filter and mirror set-up 5 suffered from the diffusion tail. It was clearly that either absorption filter or mirror caused the diffusion tail. Next step is to separate them and to see which one of them is the reason to cause diffusion tail.

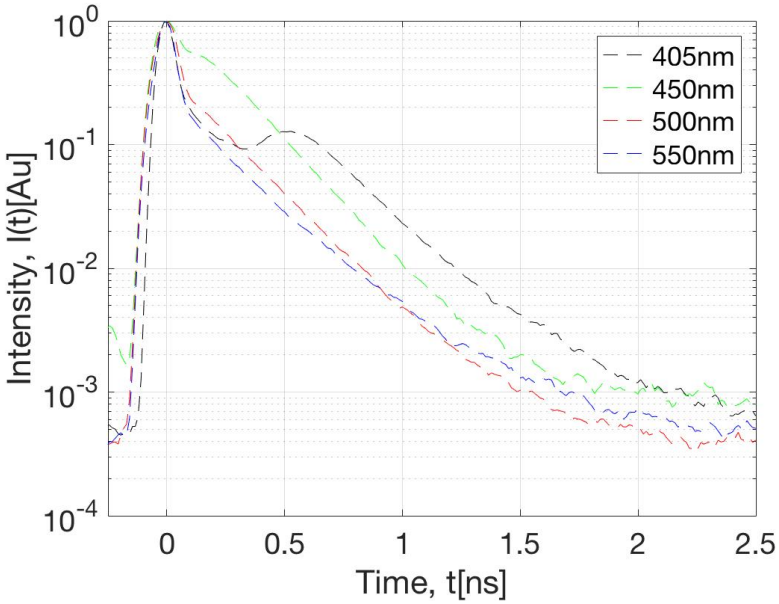

Figure 20 IRF of only absorption filter set-up 3 from 405nm to 550nm

This is the IRF of set-up 3 from 405nm to 550nm. The IRF was suffered from the diffusion tail in this kind of set-up. Compared with the IRF of set-up 4 in table 1, we can conclude that the absorption filter can cause the diffusion tail in IRF measurement. However, we still needed an optical component to cut the light down, so instead of using absorption filter, we used a pair of

polarizers. In order to test whether polarizer will also be an issue for causing diffusion tail, we built the free space set-up 3, only polarizer set-up 6 and compared the IRF of each of them.

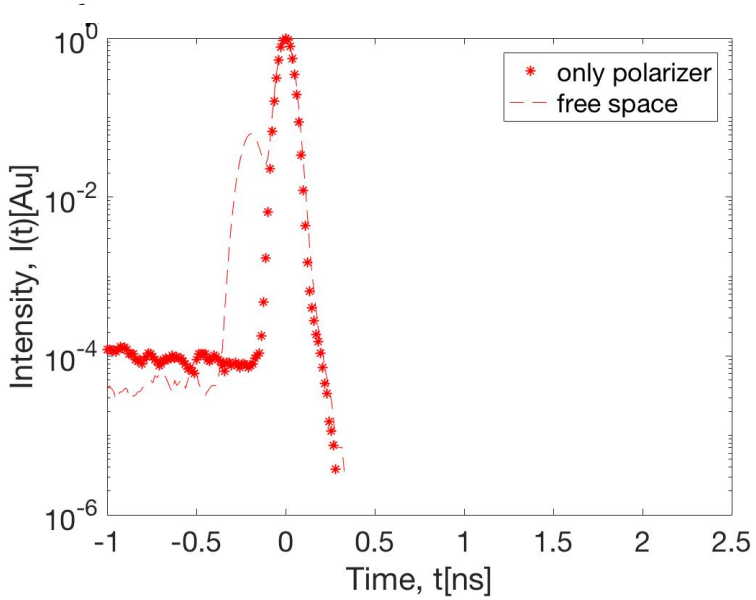

Figure 21 IRF from set-up 4 compared with IRF from set-up 6 using MPD

It turned out polarizers worked for us. The IRF of 450 collected from only polarizer set-up 6 perfectly overlapped with the data collected from free space set-up 4. The polarizers can cut the light down and also avoid the diffusion tail at the same time.

3.3.2.4 Dark count rate

Dark count rate refers to the signal of the detector that doesn't come from the laser source but from the background of the set-up. Usually, fiber probe can reduce the dark count rate as much as possible, we compared the dark count rate of set-up with fiber and without fiber.

Dark count rate		
Set-up in table 1	Detector	CFD
Set-up 7	ID100	10^1
Set-up 4	ID100	10^2
Set-up 7	MPD	10^1
Set-up 4	MPD	10^3

Table 3 The dark count rate of set up with fiber and without fiber for different detectors

From this table, it can be concluded that fiber can reduce the dark count rate of the detector. So in order to optimize the set-up, fiber have to be included in the set-up. We add the different type of fibers into polarizers and mirror set-up and see how the IRF of this set-up look like.

We stuck to 550nm wavelength and tested it with another fiber probe. One pair of polarizer is not enough for us to cut the light down, so we decided to reflected neutral density filter to cut the light intensity down, instead of absorption filter.

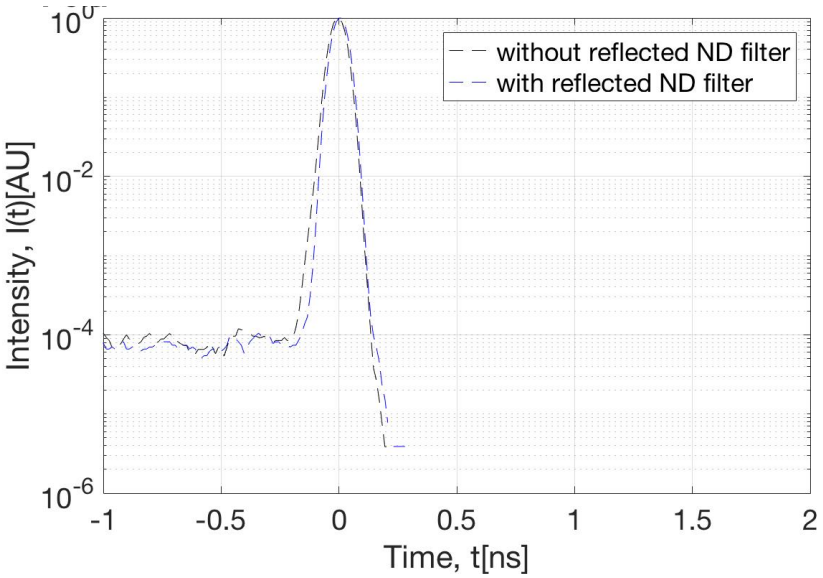

Figure 22 The IRF of set-up 8 and set-up 9 in table 1

This data was collected in order to make sure that reflected neutral density filter wouldn't cause the diffusion tail of IRF like absorption filter. It turns out, unlike the absorption filter, the reflected filter won't cause the diffusion tail.

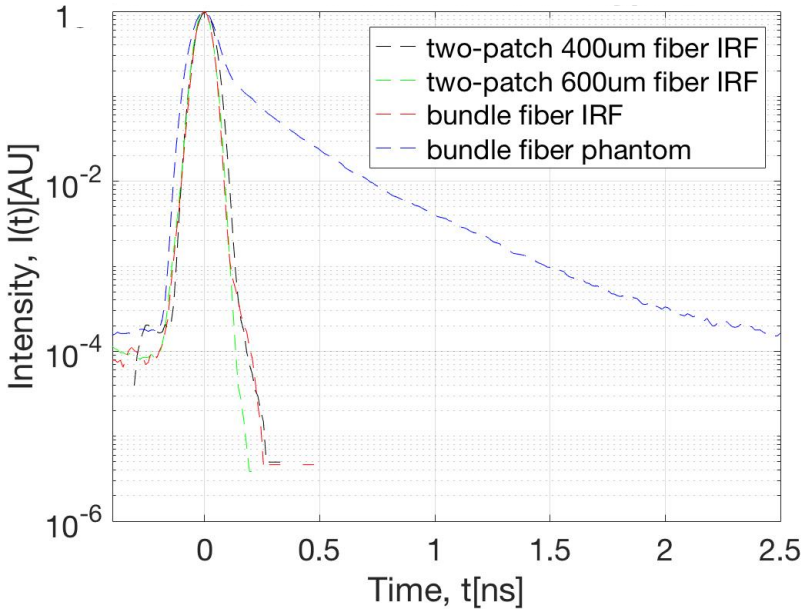

Figure 23 IRF and DTOF at 550nm from set-up 10 and set-up 11

We have two type of two-patch fibers. 400µm two-patch fiber and 600µm two-patch fiber. We test the polarizers, mirrors set-up with these different type of fibers. It seems like any type of fibers doesn't matter for IRF since the IRF of bundle fiber set-up and two-patch fiber set-up overlapped with each other.

3.3.2.5 Comparison with ID100

So after getting rid of pre-pulse, after-pulse and diffusion tail, we built the optimal set-up, which is polarizers and mirrors set-up. We want to see what the difference of IRF between MPD and ID100.

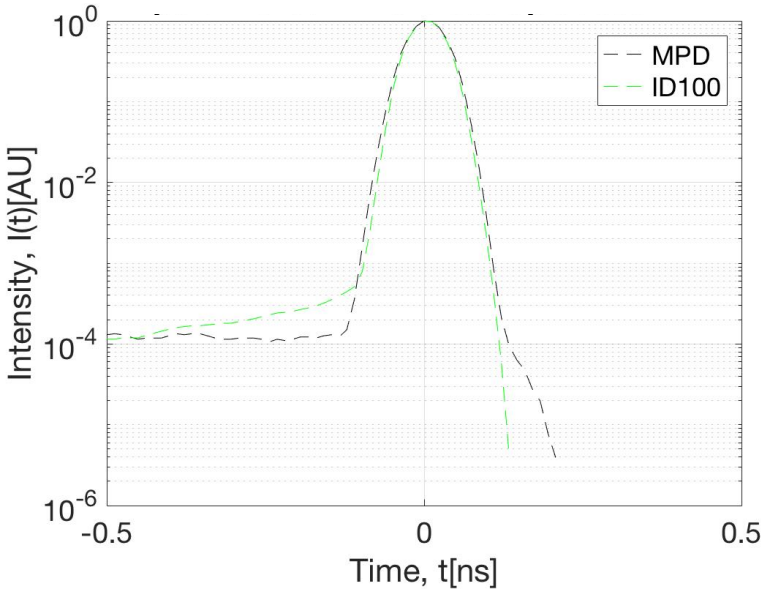

Figure 24 Comparison of IRF between the MPD and ID100 for set-up 8

This the data collected from polarizers and mirrors set-up 8 at 550nm from ID100 and MPD respectively. We can see the IRF of MPD almost overlapped with the IRF of ID100.

Although this data got rid of diffusion tail, we still want the IRF as sharp as possible and close to the pulse width of the laser. So we measured the full width half maximum(FWHM) of every IRF that is free from diffusion tail quantitatively and compared them.

Detector	Set-up in table 1	Wavelength	FWHNM(ns)
MPD	Polarizers and mirror set-up 8	405	0.0591
		450	Two peaks
		500	0.0788
MPD	Polarizer, mirrors and two-patch blue fiber set-up 10	405	0.0654
		450	0.0694
		500	0.0853
MPD	Free space set-up 4	405	0.0702
		450	0.0719
		500	0.0934
ID100	Polarizers and mirror set-up 8	450	0.0787
		500	0.0604
		550	0.0641

Table 4 FWHM of different set-up

From table 4, it can be seen that the average FWHM is around 100ps, which fit the pulse width of the laser source. The polarizer and mirror set-up FWHM is almost same the free-space set-up. From here, we can even make sure the polarizer and mirror set-up is the optimal set-up.

4. Phantom measurements

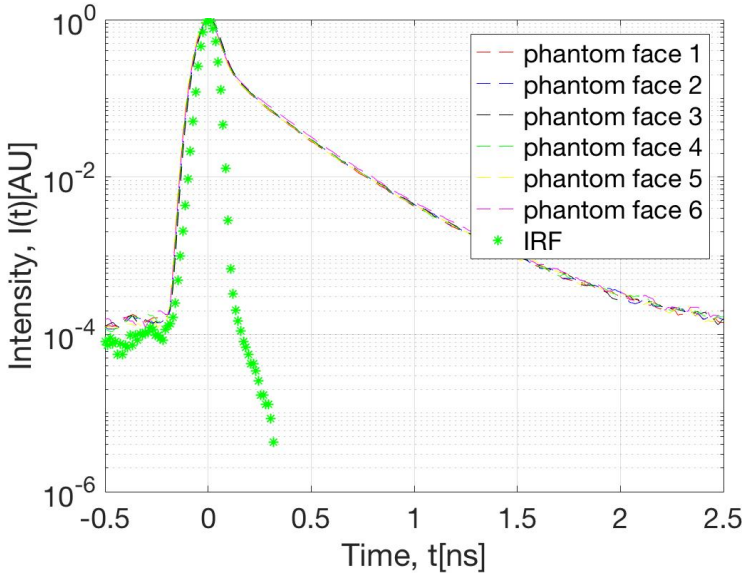

Figure 25 IRF and DTOF of polarizers, mirrors and bundle fiber set-up 11

The IRF and DTOF of the different face of the phantom from set-up 11 in table 1. Because the phantom is made of the homogenous material, diffusional reflection of different faces of phantom should look the same. The result was same with what we would expect.

Since all kind of optical components have already been tested and the set-up is optimal in respect of the optical components, it is also worthy to find the optimal result for the theory. For diffusion theory, the most important thing is to make sure the targeted media that scattering coefficient is much bigger than the absorption coefficient and also for a single photon, it will undergo many scattering events within the medium. The chance that a photon undergoes many scattering events can be increased by increasing the distance of the source probe and detector probe. However, there is also a limitation for this distance because increasing the distance will also decrease the number of remitted photons, which could cause the failure to construct DTOF of the media.

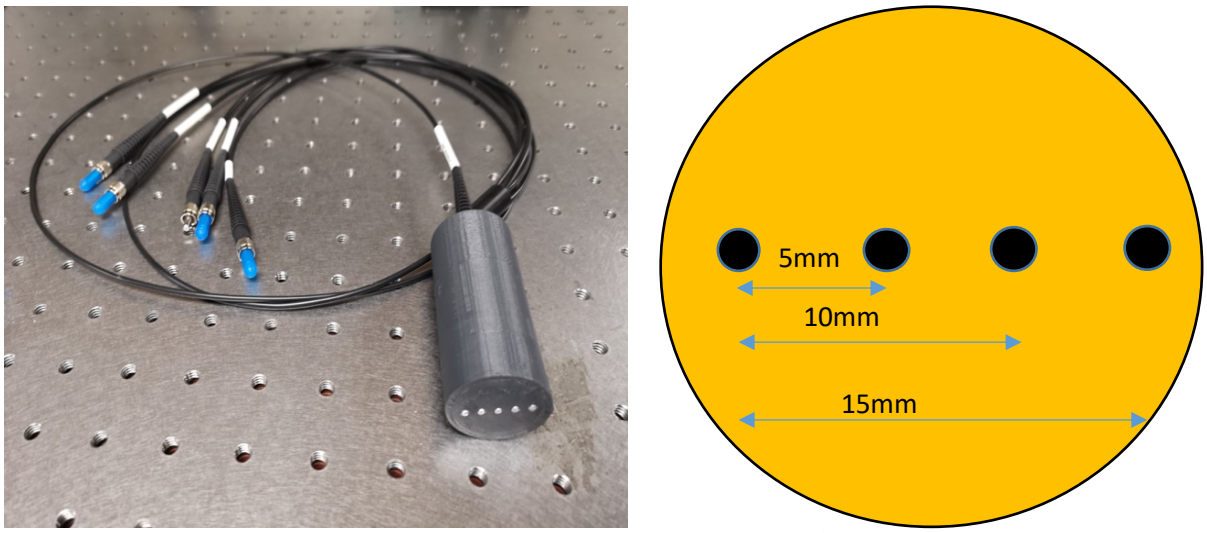

Figure 26 Black-4-channel_DRS fiber probe. Left figure shows the fiber has five fiber probes but we only used four of them in the experiment. Each fiber probe is identical with others and the diameter of them are all 400 μm.

Here, we use a fiber calls black-4-channel-DRS to control the distance between the source probe and detector probe. It includes four fiber probes and any one of them can either be a source probe or the detector probe. Each fiber probe is identical to others and the diameter of these fiber probes are 400 μm. It can have three combinations of distance between source probe and detector probe: 5mm, 10mm, 15mm.

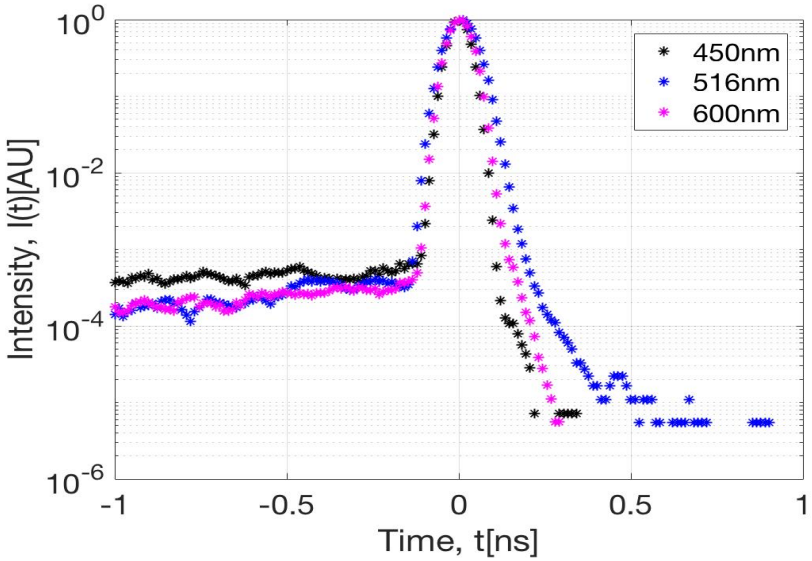

Figure 27 IRF of set-up 12 at three different wavelengths

First, we tested the IRF set-up 12 for three different wavelengths. The result fit our expectation because they almost look the same in term of the IRF.

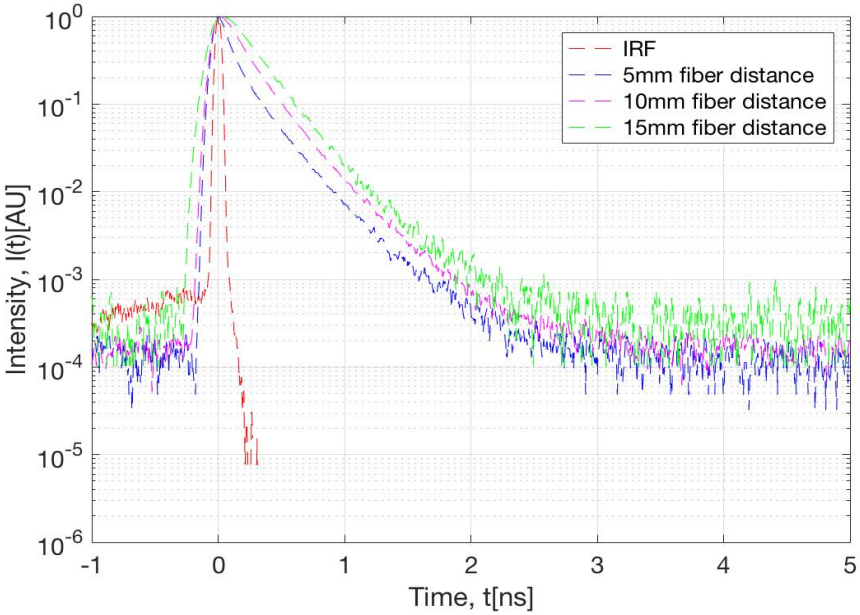

Figure 28 IRF and DTOF of set-up 12 at 550nm

Figure 28 shows the IRF and DTOF of set-up 12 at 550nm. The blue line is the grey phantom diffusion reflection for the 5mm distance between the source probe and the detector probe; the magenta line is the grey phantom diffusion reflection for the 10mm, the green line is 15mm. The result fit the expectation very well, which means for the longer of the distance between the source probe and the detector probe, the more remitted photons are scattered by the media.

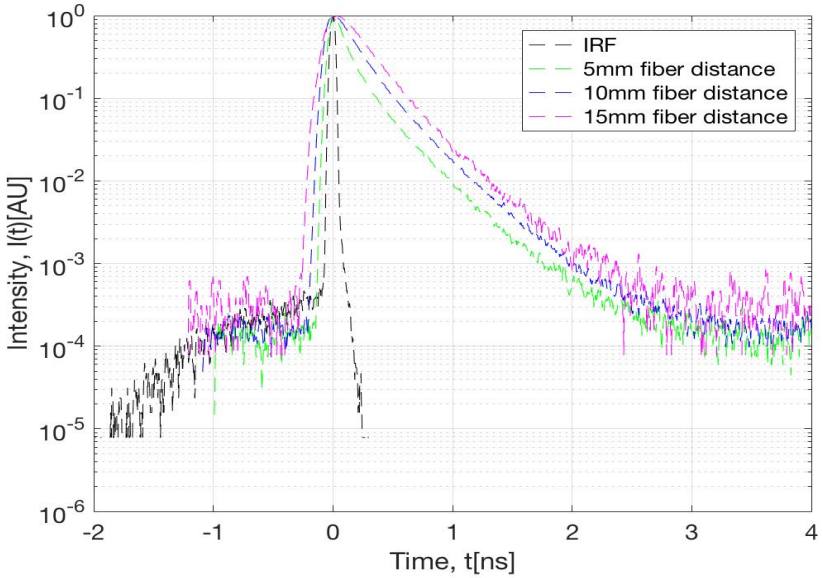

Figure 29 IRF and DTOF of set-up 12 at 600nm

This is the data for the IRF and DOTF of set-up 12 at 600nm. The data fit the expectation because for the faster distance of the fiber probe, the DOTF is more broadening.

Conclusion

By exploring the time-resolved reflectance of the phantom, it is possible to learn how the optical properties of the media can affect the reflectance of the phantom. The connection between the diffusion theory and experiment part are strong and they can effect each other. In order to get the optimal DTOF measurement from TCSPC system, it is also necessary to build different set-ups and test different media. Even though the optical properties of media are unknown, there are still some expectations for media with different optical properties. By testing and comparing the result with the expectation, the optimal set-up can be built. We have built the set-up with different optical components and detectors. By comparison the IRF of different set-up, we knew that the diffusion tail can caused by the absorption filter and also the detectors itself.

The diffusion tail of IRF caused by absorption filter should be avoided in the reflectance measurement. Eventually, the set-up with optical components polarizers, mirrors and fiber worked. The DTOF measurement of surface of solid phantom based on this set-up fit the expectation. For different faces of solid phantom, the DTOF all look the same. Also, the diffusion theory mainly fit the DTOF of solid phantom. Here is the table for prediction of optical properties of the solid phantom.

Wavelength (nm)	Fiber probe distance (cm)	$\mu_a(cm^{-1})$	$\mu_s'(cm^{-1})$
550	0.5	0.05	20
550	1.0	0.11	14
550	1.5	0.08	5.5
600	0.5	0.05	21
600	1.0	0.085	12
600	1.5	0.08	6

Table 5 Data fitting for solid phantom

We expected that for same wavelength measurement, even with different fiber probe distance, the optical properties of the solid phantom would be the same and compared with the shorter of the wavelength, both absorption coefficient and scattering coefficient of longer wavelength would go down. The difference between the theoretical prediction and expectation could came from the fact that the fiber probe could not be considered as totally collimated pencil beam or the fiber probe was not placed vertically on the surface of the phantom. It is also possible that only for some fiber probe distances, the diffusion theory worked well. Or it could be that the phantom inside is not totally homogenous but the surface is homogenous. Eventually, we showed that based on this set-up, we can extract the optical properties of a medium by time-resolved reflectance measurement.

Future work

In the future, instead of getting the IRF from the specular reflection of the white puck, we will get the IRF by measuring the specular reflection of a piece of glass. Also, the diffraction caused by the polarizers will also need to be eliminated. Besides, we can make several liquid phantoms with different scattering coefficients and absorption coefficients and test them to see how the results fit with the true optical properties of the liquid phantom. Besides, we can use different theories to fit the data and see what the difference between these theories.

List of Acronyms

APD	avalanche photodiode
CFD	constant fraction discriminator
DTOF	distribution of time of flight
EBC	extrapolated boundary condition
FWHM	full width at half maximum
IRF	instrument response function
ND	neutral density
PMT	photomultiplier tube
SPAD	single-photon avalanche diode
SYNC	synchronization
TCSPC	time-correlated single photon counter
TR	time resolved
ZBC	zero boundary condition

Reference

1. Lihong V. Wang, H.-i.W., *Biomedical Optics Principles and Imaging* 1ed. 2007: Wiley-Interscience. 376.
2. Ashley J. Welch, *Optical-Thermal Response of Laser-Irradiated Tissue* Second Edition ed. 2011: Springer.
3. Ishimaru, A., *Diffusion of Light in Turbid Material.* Applied Optics, 1989. **28**(12): p. 2210-2215.
4. Torricelli, A., et al., *Time domain functional NIRS imaging for human brain mapping.* Neuroimage, 2014. **85** (1): p. 28-50.
5. Bargo, P.R., et al., *In vivo determination of optical properties of normal and tumor tissue with white light reflectance and an empirical light transport model during endoscopy.* J Biomed Opt, 2005. **10**(3): p. 034018.
6. Patterson, M.S., B. Chance, and B.C. Wilson, *Time resolved reflectance and transmittance for the non-invasive measurement of tissue optical properties.* Appl Opt, 1989. **28**(12): p. 2331-6.
7. Alayed, M. and M.J. Deen, *Time-Resolved Diffuse Optical Spectroscopy and Imaging Using Solid-State Detectors: Characteristics, Present Status, and Research Challenges.* Sensors (Basel), 2017. **17**(9): p. 2115.
8. Doornbos, R.M., et al., *The determination of in vivo human tissue optical properties and absolute chromophore concentrations using spatially resolved steady-state diffuse reflectance spectroscopy.* Phys Med Biol, 1999. **44**(4): p. 967-81.
9. Wang, A.M., et al., *Depth-sensitive reflectance measurements using obliquely oriented fiber probes.* J Biomed Opt, 2005. **10**(4): p. 44017.
10. Kienle, A., et al., *Spatially resolved absolute diffuse reflectance measurements for noninvasive determination of the optical scattering and absorption coefficients of biological tissue.* Appl Opt, 1996. **35**(13): p. 2304-14.
11. Antonio Pifferi, A.T., Paola Taroni, Daniela Comelli, Andrea Bassi, and Rinaldo Cubeddu *Fully automated time domain spectrometer for the absorption and scattering characterization of diffusive media.* Review of scientific instruments, 2007. **78**(5): p. 053101.
12. Pavia, J.M., *Near-Infrared Optical Tomography With Single-Photon Avalanche Diode Image Sensors.* 2015.
13. Becker, W., *The bh TCSPC handbook* 2014: Becker & Hickl, 2012.
14. Homma, S., et al., *Near-infrared estimation of O-2 supply and consumption in forearm muscles working at varying intensity.* Journal of Applied Physiology, 1996. **80**(4): p. 1279-1284.
15. Van Houten, J.P., et al., *Imaging brain injury using time-resolved near infrared light scanning.* Pediatr Res, 1996. **39**(3): p. 470-6.
16. Vishwanath, K., *computational modeling of time-resolved fluorescence transport in turbid media for noninvasive clinical diagnostics*, in *University of Michigan*. 2005: Thesis in Applied Physics Program. p. 67.

17. Laidevant, A., et al., *Effects of the surface boundary on the determination of the optical properties of a turbid medium with time-resolved reflectance.* Appl Opt, 2006. **45**(19): p. 4756-64.
18. Thomas J. Farrell, M.S.P., *A diffusion theory model of spatially resolved, steady-state diffuse reflectance for the noninvasive determination of tissue optical properties in vivo.* Med.Phys, 1992. **19**(4): p. 879-888.
19. Kienle, A. and M.S. Patterson, *Improved solutions of the steady-state and the time-resolved diffusion equations for reflectance from a semi-infinite turbid medium.* J Opt Soc Am A Opt Image Sci Vis, 1997. **14**(1): p. 246-54.
20. Swartling, J., et al., *Dynamic time-resolved diffuse spectroscopy based on supercontinuum light pulses.* Appl Opt, 2005. **44**(22): p. 4684-92.
21. Bassi, A., et al., *Portable, large-bandwidth time-resolved system for diffuse optical spectroscopy.* Optics Express, 2007. **15**(22): p. 14482-14487.
22. M. Mazurenka, A.J., H. Wabnitz, D. Contini, L. Spinelli, A. Pifferi, R. Cubeddu, A. Dalla Mora, A. Tosi, F. Zappa, and R. Macdonald1, *Non-contact time-resolved diffuse reflectance imaging at null source-detector separation.* Optical Express, 2011. **20**(1): p. 283-290.
23. H.A. García, D.I.I., J.A. Pomarico, D. Grosenick, R. Macdonald *Retrieval of the optical properties of a semiinfinite compartment in a layered scattering medium by single-distance, time-resolved diffuse reflectance measurements.* Journal of Quantitative Spectroscopy & Radiative Transfer, 2016.
24. Pifferi, A., et al., *Time-resolved diffuse reflectance using small source-detector separation and fast single-photon gating.* Physical Review Letters, 2008. **100**(13): p. 138101.
25. Alayed, M. and M.J. Deen, *Time-Resolved Diffuse Optical Spectroscopy and Imaging Using Solid-State Detectors: Characteristics, Present Status, and Research Challenges.* Sensors (Basel), 2017. **17**(9).
26. Andersson-Engels, S., et al., *Multispectral tissue characterization with time-resolved detection of diffusely scattered white light.* Opt Lett, 1993. **18**(20): p. 1697-9.
27. Bassi, A., et al., *Time-resolved spectrophotometer for turbid media based on supercontinuum generation in a photonic crystal fiber.* Optics Letters, 2004. **29**(20): p. 2405-2407.
28. Wahl, M., *Time-Correlated Single Photon Counting*. 2014: PICOQUANT.
29. Becker, W., *Correlartion Measurements by Advanced TCSPC Techniques*, B.H. GmbH, Editor. 2002.
30. Becker, W., *TCSPC Performance of the id100-50 Detector* 2005.